Electronic Supplementary Information

Assessing the environmental benefit of palladium-based single-atom heterogeneous catalysts for Sonogashira coupling

D. Faust Akl,[a] D. Poier,[b] S.C. D'Angelo,[a] T.P. Araújo,[a] V. Tulus,[a] O.V. Safonova,[c] S. Mitchell,[a] R. Marti,[b] G. Guillén-Gosálbez,[a] and J. Pérez-Ramírez[a]

[a] Institute for Chemical and Bioengineering, Department of Chemistry and Applied Biosciences, ETH Zurich, Vladimir-Prelog-Weg 1, 8093 Zürich, Switzerland.

[b] Institute of Chemical Technology, University of Applied Sciences and Arts of Western Switzerland Fribourg, Boulevard de Pérolles 80, 1700 Fribourg, Switzerland.

[c] Paul-Scherrer-Institute, Forschungsstrasse 111, 5232 Villigen PSI, Switzerland.

Note S1. Supplementary experimental details

Catalyst preparation

Preparation of catalyst carriers. Activated carbon (AC, Norit Rox 0.8) was used as a fine powder (sieve fraction <0.2 mm). High-purity, high-surface-area γ-Al_2O_3 (Puralox SCFa-140, Sasol) was calcined at 973 K (5 h, 5 K min^{-1}) in static air before further use. As the first step of nitrogen incorporation, AC (Norit Rox 0.8, sieve fraction 0.2-0.4 mm) was refluxed in 20 cm^3 concentrated nitric acid (>65 wt.%, Sigma-Aldrich, puriss.) per gram of carbon at 353 K for 16 h. The mixture was poured into ice-cooled DI water, filtered, washed copiously with DI water (1 dm^3 g_{AC}^{-1}), and dried overnight (338 K). The acid-activated carbon was mixed with dicyandiamide (99 %, Sigma-Aldrich, 3 g g_{AC}^{-1}) and acetone (*ca.* 30 cm^3 g_{AC}^{-1}), which was subsequently evaporated (353 K) under constant stirring. Lastly, the dried solid was gently crushed, transferred to ceramic boats and carbonised in flowing nitrogen (723 K, 3 h hold, then 923 K, 2 h hold, all ramps 5 K min^{-1}), and nitrogen-doped carbon (NC) was obtained.[1] Graphitic carbon nitride prepared through the condensation-polymerisation of dicyandiamide (823 K, 4 h, 2.3 K min^{-1} ramp) was ball-milled (6 repetitions of 5 min at 35 Hz, 30 s at 5 Hz) and exfoliated in static air (773 K, 10 h hold, 5 K min^{-1} ramp) to obtain exfoliated carbon nitride (ECN).[2]

Preparation of Pd/NC, Pd/ECN, and Pd/Al_2O_3 SACs. An appropriate amount (0.5 wt.% nominal palladium loading) of $(NH_3)_4Pd(NO_3)_2$ (5 wt.% solution in water, abcr) and DI water (15 cm^3) were added to a sonicated (30 min) suspension of the catalyst carrier (1 g of NC, ECN, or Al_2O_3 in 20 cm^3 DI water) and vigorously stirred overnight. The suspension was subjected to repeated cycles (20) of microwave irradiation (100 W for 15 s) with intermittent cooling, separated through centrifugation, and washed with water (50 cm^3, 5 times) and ethanol. The obtained solids were dried overnight (338 K) and annealed in a tubular oven under nitrogen flow (573 K, 5 h hold, 5 K min^{-1} ramp).

Preparation of Pd/AC SAC. $PdCl_2$ (99.9 %, Strem Chemicals) was dissolved in aqua regia (1.5 cm^3) and added dropwise to the AC carrier while mixing the paste with a plastic spatula. The obtained solids were dried and annealed in nitrogen as described above.

Preparation of bimetallic PdCu/NC SAC. The as-prepared palladium catalyst (Pd/NC, 1 g), $Cu(NO_3)_2 \cdot 2.5\ H_2O$ (98 %, Acros Organics) and ethanol (*ca.* 2 cm^3) were mixed mechanically into a thick paste, dried and annealed in nitrogen as described above.

Catalyst characterisation

Powder X-ray diffractograms were acquired in a PANalytical X'Pert PRO-MPD instrument (Bragg-Brentano geometry) using a Ni-filtered Cu Kα source. Data was collected at 2θ in the range of 3-60° with a step size of 0.08° and a collection time of 162 s. Nitrogen sorption isotherms (77 K) were acquired using a Micromeritics TriStar instrument and argon sorption was conducted (77 K) with a Micromeritics TriFlex analyser over previously degassed specimens (8 h, 423 K, vacuum). The composition of the carbon carriers (C, H, N, O) was determined using a LECO CHN-900 elemental analyser equipped with an infrared spectrometer. The analysis of the metal content with inductively coupled plasma optical emission spectroscopy was conducted in a Horiba Ultra 2 instrument (photomultiplier tube detector). Sample aliquots (15 mg) were loaded into polytetrafluoroethylene tubes, to which a mixture (3:1, 2 cm^3) of nitric acid (>65 wt.%, Sigma-Aldrich) and hydrogen peroxide (30 wt.%, Sigma-Aldrich) was slowly added. Alumina-containing samples were digested with a mixture of phosphoric, sulfuric, and hydrofluoric acids. The capped tubes were heated (473 K, 20 min) in a microwave reactor (Turbowave) under elevated nitrogen pressure (48 bar). Liquid organic samples were dried (338 K) and carbonised with the abovementioned hydrogen peroxide-nitric acid mixture with added sulfuric acid (1 cm^3, >95%, Sigma-Aldrich). The obtained solutions were diluted with MilliQ water and solids were removed through PTFE syringe filters (0.25 μm pore size). Quantification was based on the emission intensity at 340.46 nm (Pd) and 324.75 nm (Cu) averaged over three measurements. X-ray photoelectron spectroscopy was conducted on a Physical Electronics Instruments Quantum 2000 instrument with monochromatic Al Ka radiation (15 kV, 32.3 W). The spectral acquisition occurred under ultrahigh vacuum conditions ($5 \cdot 10^{-8}$ Pa residual pressure) with a pass energy of 46.95 eV. All XPS signals were referenced using the C1 *s* photoemission which was set at 284.8 eV. Peak fitting with reference spectra[3-7] was conducted using the CasaXPS software.[8] For scanning transmission electron microscopy (STEM) the samples were dusted onto standard carbon-film copper and nickel grids (300 mesh). High-angle annular dark-field (HAADF) STEM and energy dispersive X-ray spectroscopy (EDX) was performed on a FEI Talos F200X microscope with a SuperX detector (200 kV acceleration potential). Image frames of 512 by 512 pixels were acquired under varying dwell times (35-74 μs). EDX elemental maps were averaged over 20 frames in the spectral range up to 20 keV, and post-processed (background subtraction and Gaussian blur). Aberration corrected annular dark-field STEM (AC-ADF-STEM) images of as-prepared and used catalysts were acquired on a Hitachi HD-2700CS instrument operated at 200 kV. X-ray absorption

spectroscopy (XAS) was conducted at the X10DA (SuperXAS) beamline of the Swiss Light Source. The X-ray beam from the 2.9 T superbend was collimated using a Pt-coated mirror, monochromatised using a Si(111) channel-cut monochromator, and focused to a spot size of 500×100 μm (horizontal×vertical) using a Pt-coated toroidal mirror. Data were acquired from pressed pellets at the Pd and Cu *K*-edge in transmission mode, using three 15 cm long Ar/N_2-filled ionisation chambers. The samples were placed between the first and the second ionisation chamber. For the absolute energy calibration, a metallic (Pd, Cu) foil was measured simultaneously between the second and third ionisation chambers. The resulting spectra were energy calibrated, background corrected and normalised using the Athena program from the Demeter software suite.[9] EXAFS fitting was performed using the parameters described in Table S4.

Catalyst evaluation

Chemicals. All chemicals were acquired from Chemie Brunschwig AG and Merck and used without further purification.

Sonogashira coupling reaction. Aside from the SACs, the following benchmark systems were included in the catalytic tests: Pd_{NP}/C (10 wt.% palladium content, Sigma-Aldrich, Lot MKBV2219V), $PdCl_2(P(C_6H_5)_3)_2$ (Acros Organics), $Pd(P(C_6H_5)_3)_4$) (Sigma-Aldrich), and $Pd(CH_3COO)_2$ (Acros Organics). Unless otherwise stated, the Sonogashira coupling reaction was performed following a standard procedure: a degassed solution consisting of iodobenzene (1 equivalent, eq.), phenylacetylene (1.1 eq.), base (2.2 eq.), 1,3,5-trimethylbenzene (0.25 eq., internal standard), and solvent (0.5 M) was added to the palladium catalyst (0.1 mol%, 0.5 wt.% palladium content for SAC), copper(I) iodide (1 mol%), and ligand (1 mol%), and vigorously stirred for 24 h at 353 K under a protective atmosphere (Ar). After cooling to room temperature, the SAC was separated from the reaction mixture by filtration, washed three times with acetonitrile (3 cm^3) and ethyl acetate (3 cm^3), and dried under reduced pressure. The reaction solution was analysed by gas chromatography (GC), performed on a Thermo TRACE 1300 chromatograph equipped with a flame ionisation detector, and a ZB-5 column (5%-phenyl-95%-Dimethylpolysiloxane, 30 m length, 0.25 mm inner diameter, 0.25 μm film thickness) using helium as carrier gas (see Note S2, Fig. S11).

Note S2. Experimental procedure under standard conditions

A degassed solution of iodobenzene (30.0 mmol), phenylacetylene (33.4 mmol), triethylamine (66.4 mmol), 1,3,5-trimethylbenzene (7.61 mmol), and acetonitrile (60 cm^3) was added to a glass vial containing solid SAC (623 mg, 0.5 wt.% palladium content), copper(I) iodide (58.9 mg), and triphenylphosphine (80.9 mg), and vigorously stirred for 24 h at 353 K under a protective atmosphere (argon). After cooling to room temperature, the catalyst was separated by filtration, washed three times with acetonitrile (10 cm^3) and once with ethyl acetate (10 cm^3), and dried under reduced pressure. Volatile compounds were removed from the reaction solution filtrate under reduced pressure at elevated temperature (353 K), the residue was treated with ethyl acetate, washed three times with water, and dried over sodium sulphate. Finally, the solvent was removed under reduced pressure with subsequent purification of the obtained residue by flash column chromatography (Combiflash Rf+, heptane eluent) equipped with a UV detector and silica gel columns (RediSep Rf+, 35-70 μm average particle size). Diphenylacetylene was obtained as a colourless crystalline solid (3.16 g, 17.7 mmol, 59%). The yield determined through gas chromatography (GC) was 62% (representative chromatogram in Fig. S11).

Note S3. Product isolation

Volatile substances were removed from the reaction solution under reduced pressure, the residue was treated with ethyl acetate, washed three times with water and dried over sodium sulfate. Finally, solvent removal under reduced pressure with subsequent purification of the residue by flash column chromatography using a Combiflash Rf+ equipped with a UV detector and RediSep Rf+ columns (silica gel 60, 230-400 mesh, 35-70 μm average particle size) yielded diphenylacetylene as colourless, crystalline solid. ^{1}H-NMR spectra were recorded with a Bruker 300 Ultrashield spectrometer and referenced against the chemical shift of the residual protic-solvent peak ($CDCl_3$: 7.26 ppm); for ^{13}C-NMR spectra the deuterated solvent peak ($CDCl_3$: 77 ppm) was used (see Fig. S12-S15).

Iodobenzene (1)

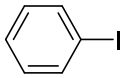

^{1}H NMR (300 MHz, $CDCl_3$): δ [ppm] = 7.71 (2H, m, *o*-H), 7.33 (1H, m, *p*-H), 7.11 (2H, m, *m*-H).
^{13}C NMR (75 MHz, $CDCl_3$): δ [ppm] = 137.6, 130.4, 127.6, 94.5.

Ethynylbenzene (2)

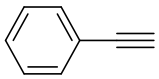

^{1}H NMR (300 MHz, $CDCl_3$): δ [ppm] = 7.50 (2H, m, *o*-H), 7.33 (3H, *m*-H and *p*-H), 3.07 (1H, s, Ph–CC–*H*).
^{13}C NMR (75 MHz, $CDCl_3$): δ [ppm] = 132.3, 128.9, 128.5, 122.3, 83.8, 77.3.

1,2-Diphenylethyne (3)

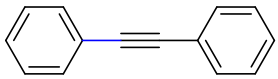

^{1}H NMR (300 MHz, $CDCl_3$): δ [ppm] = 7.54 (4H, m), 7.35 (6H, m).
^{13}C NMR (75 MHz, $CDCl_3$): δ [ppm] = 131.8, 128.5, 128.4, 123.4, 89.52.

1,4-Diphenylbuta-1,3-diyne (4)

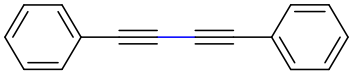

^{1}H NMR (300 MHz, $CDCl_3$): δ [ppm] = 7.53 (m, 4H), 7.35(m, 6H).
^{13}C NMR (75 MHz, $CDCl_3$): δ [ppm] = 132.7, 129.4, 128.6, 122.0, 81.7, 74.1.

Table S1. Environmental impact metrics associated to CuI use and wastewater treatment determined by LCA.

Impact	GWP[a] / $ton_{CO_2\text{-eq}}$ $ton_{(3)}$	HH[b] / DALY $ton_{(3)}^{-1}$	EQ[c] / species-yr $ton_{(3)}^{-1}$	Res[d] / USD_{2013} $ton_{(3)}^{-1}$
Organometallic complex (homogeneously-catalysed process)				
CuI use	$4.27 \cdot 10^{-2}$	$4.49 \cdot 10^{-4}$	$7.71 \cdot 10^{-7}$	5.71
Wastewater treatment	$7.70 \cdot 10^{-3}$	$4.57 \cdot 10^{-4}$	$-1.10 \cdot 10^{-7}$	$4.65 \cdot 10^{1}$
SAC (heterogeneously-catalysed process)				
CuI use	$4.71 \cdot 10^{-2}$	$4.95 \cdot 10^{-4}$	$8.50 \cdot 10^{-7}$	6.29
Wastewater treatment	$8.10 \cdot 10^{-3}$	$4.80 \cdot 10^{-4}$	$-1.16 \cdot 10^{-7}$	$4.89 \cdot 10^{1}$

Metrics quantifying impact per ton of product **3**: [a]Midpoint Global Warming Potential in tons of CO_2 equivalents ($ton_{CO_2\text{-eq}}$). [b]Endpoints Human Health in disability-adjusted life years (DALYs). [c]Ecosystems Quality in local species loss per year (species-yr). [d]Resources (Res) in USD (USD_{2013}).

Table S2. Bulk composition of as-prepared catalysts.

Catalyst	w_B(Pd)[a] / wt.%	Elemental composition[b]
Pd/Al_2O_3	0.10	-
Pd/ECN	0.35	$C_{29.0}H_{0.1}N_{67.3}O_{3.7}$
Pd/AC	0.40	$C_{95.0}H_{0.1}N_{0.5}O_{4.0}$
Pd/NC	0.48-0.64	$C_{86.0}N_{3.0}O_{11.0}$
PdCu/NC	0.53 (2.66)[c]	$C_{85.0}N_{3.5}O_{11.5}$

[a]Bulk palladium content determined through ICP-OES. A nominal palladium loading of 0.5 wt.% was targeted in all cases. [b]CHNO analysis of the carrier. [c]Copper content in brackets.

Table S3. Elemental surface composition of as-prepared and used Pd SACs determined by XPS.

Catalyst	Pd / at.%	Cu / at.%	C / at.%	N[a] / at.%	O / at.%	P / at.%	I / at.%
Pd/AC	0.12	-	90.8	0.9	6.8	-	-
Pd/AC-R1	0.09	0	91.5	1.5	6.2	0.1	0.1
Pd/ECN	0.10	-	42.4	56.4	1.1	-	-
Pd/ECN-R1	0.13	0.1	42.0	56.5	1.4	0.1	0
Pd/NC	0.17	-	87.4	9.5	3.0	-	-
Pd/NC-R1	0.14	0.1	87.4	10.7	4.1	0.1	0.5
Pd/NC-R2	0.15	0.2	84.4	10.4	4.5	0	0.5
Pd/NC-R3	0.10	0.2	84.5	9.9	4.7	0.1	0.5
PdCu/NC	0.18	0.4	84.5	6.6	7.8	-	-
PdCu/NC-R1	0.13	0.1	85.9	6.4	7.2	0.1	0.2
Catalyst	Pd / at.%	Cu / at.%	C / at.%	Al / at.%	O / at.%	P / at.%	I / at.%
Pd/Al_2O_3	0.03	-	3.9	[a]51.4	44.3	-	-
Pd/Al_2O_3-R1	0	0	10.6	[a]48.5	40.1	0.1	0

Notably, the surface composition revealed a higher palladium content than in the bulk, likely owing to the preferred surface localisation using the presented synthesis method. Furthermore, for PdCu/NC the surface Cu:Pd molar ratio was different (around 2:1) than the bulk composition, which is associated with a distinct localisation of the copper precursor (e.g., in the micropores).

Table S4. EXAFS fitting parameters and results of as-prepared and used Pd SACs.

Catalyst	Coordination shell[a]	Coordination number / -	σ^{2c} / Å^2	R^d / Å	$R_{ref}{}^e$ / Å	$\Delta E_0{}^f$ / eV
Pd/NC	Pd-O/N	2.3 ± 0.4	0.002 ± 0.002	1.97 ± 0.01	2.06	4.59 ± 1.74
Pd/NC-R1	Pd-O/N	2.4 ± 0.5	0.004 ± 0.003	1.97 ± 0.02	2.06	3.12 ± 2.32
	Pd-I	0.4 ± 0.6	0.007 ± 0.015	2.59 ± 0.08	2.65	
Pd/NC-R3	Pd-O/N	2.4 ± 0.5	0.003 ± 0.003	1.97 ± 0.02	2.06	2.37 ± 2.26
	Pd-I	0.3 ± 0.5	0.004 ± 0.012	2.59 ± 0.06	2.65	
PdCu/NC	Pd-O/N	2.2 ± 0.3	0.002 ± 0.002	1.97 ± 0.01	2.06	4.41 ± 1.71
	Cu-O/N	2.6 ± 0.2	0.008 ± 0.002	1.91 ± 0.01	2.12	3.16 ± 1.15

[a]Fourier-transform parameters: k = 3-12 Å^{-1}, R = 1-3 Å. Amplitude attenuation factors: $S_{0,Pd}{}^2$ = 0.82, $S_{0,Cu}{}^2$ = 0.885. [c]Debye-Waller factor. [d]Coordination distance. [e]Coordination distance in reference material. [f]Energy shift.

Table S5. Copper content in the as-prepared and used NC-based Pd SACs.

Catalyst[a]	w_B(Cu)[b] / wt.%	
	Pd/NC	PdCu/NC
R0	0	2.4
R1	1.8	0.5
R2	1.0	0.6
R3	1.5	-

[a]R*X* with *X* the number of catalytic runs conducted with the catalyst. [b]Bulk copper content determined by ICP-OES.

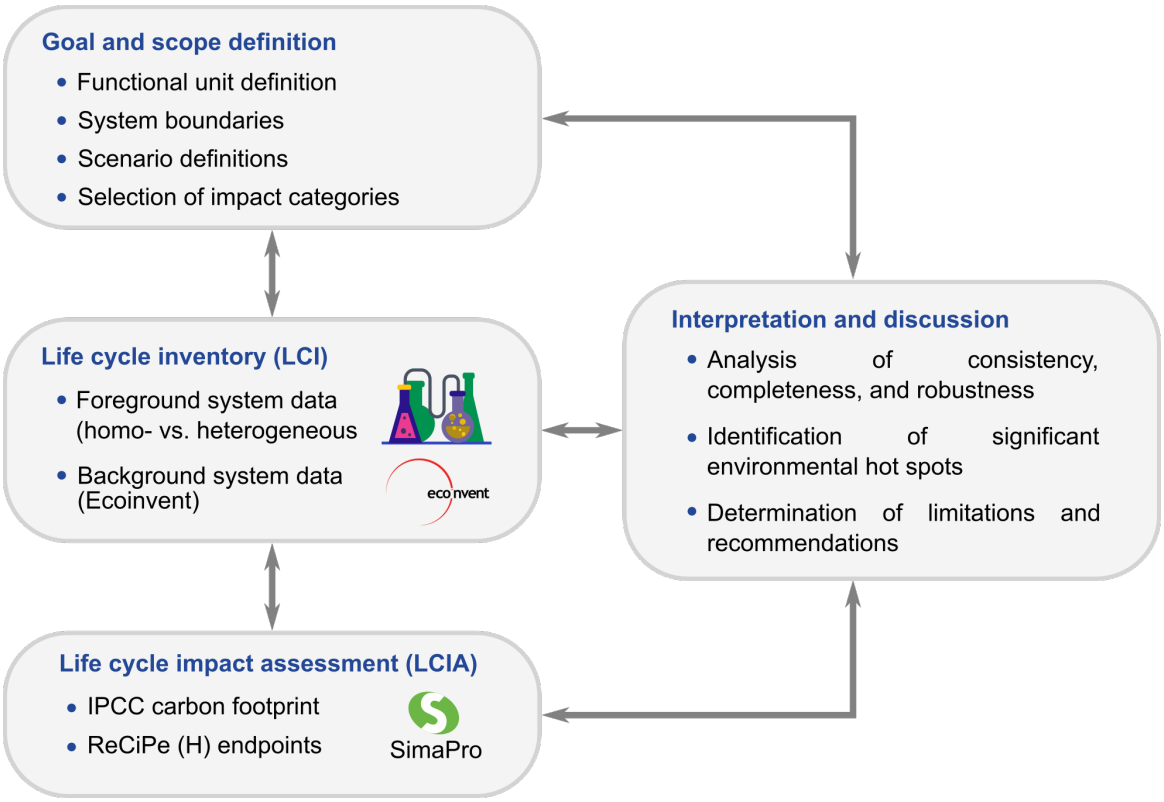

Fig. S1. Schematic representation of the steps comprising life cycle assessment.[10]

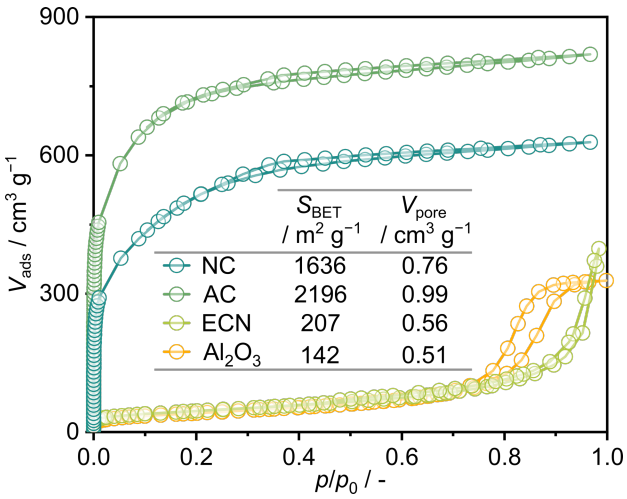

Fig. S2. Gas sorption isotherms of the catalyst supports collected at 77 K with corresponding BET surface areas (S_{BET}) and pore volumes (V_{pore}) shown in the table inset. Argon was used instead of nitrogen for the microporous activated carbon (AC) and nitrogen-doped carbon (NC) supports. Alumina (Al_2O_3) and exfoliated graphitic carbon nitride (ECN) displayed isotherm characteristic of mesoporous materials.

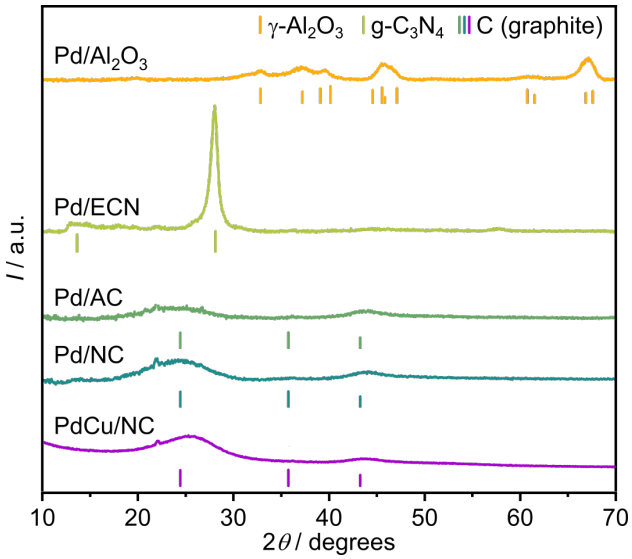

Fig. S3. Powder X-ray diffraction patterns of the as-prepared Pd and PdCu single-atom catalysts (SACs) displaying characteristic reflections of the carrier materials (vertical lines indicate reference patterns). The absence of sharp reflections in AC and NC confirms their amorphous nature. The Al_2O_3 support showed reflections characteristic of its gamma polymorph; the low intensity agrees with the small crystallite sizes observed by high-angle annular dark field scanning transmission electron microscopy (HAADF-STEM). ECN displayed reflections characteristic of the stacked graphitic basal planes of graphitic carbon (g-C_3N_4). No reflections corresponding to the bulk metal phase were evidenced in any of the catalysts, consistent with their atomically dispersed character.

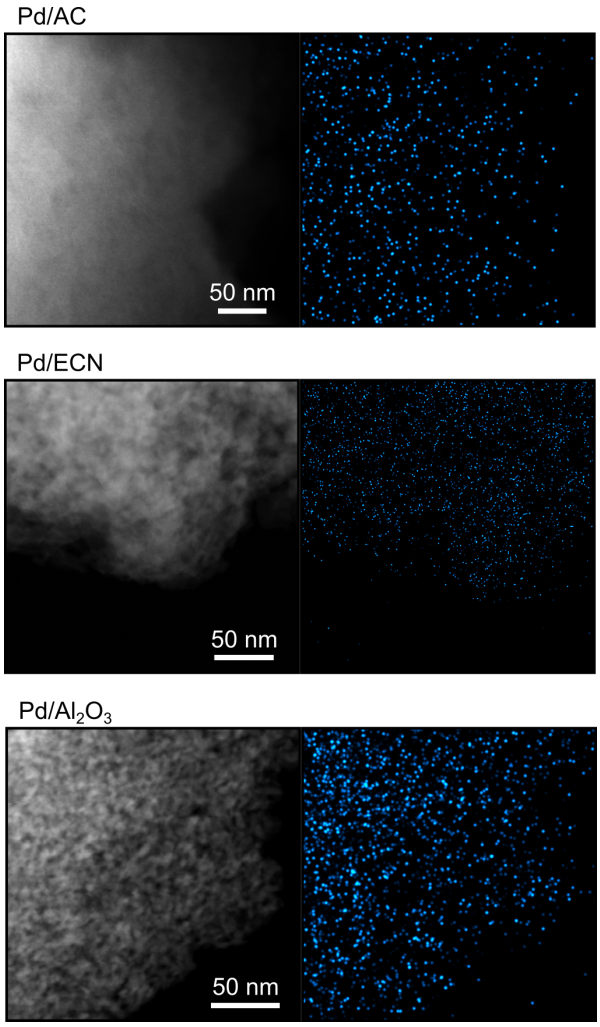

Fig. S4. High-angle annular dark field scanning transmission electron microscopy (HAADF-STEM) images and corresponding energy-dispersive X-ray spectroscopy (EDX) maps of the as-prepared Pd SACs. No palladium nanoparticles were visible in the HAADF-STEM images and the elemental maps confirm the uniform distribution of palladium species over the carriers.

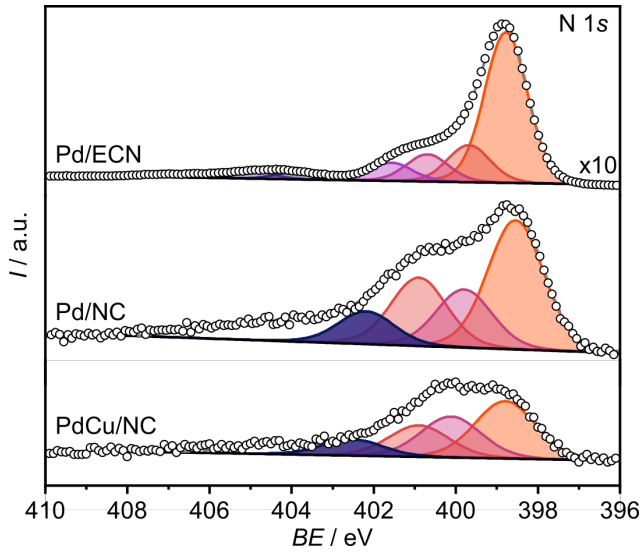

Fig. S5. N 1*s* X-ray photoelectron spectroscopy (XPS) spectra of the as-prepared Pd SACs based on NC and ECN with overlaid spectral fit. The high nitrogen content present in Pd/ECN could be mainly attributed to aromatic ring nitrogen (398.8 eV) and tertiary nitrogen (399.8 eV) present in the tris-triazine sub-units of the scaffold. A contribution of NH_x-groups can be assigned to defects due to unpolymerised nitrile groups (400.7 eV).[11,12] Both Pd/NC and PdCu/NC displayed qualitatively similar spectra. They could be fitted through components assigned to pyridinic nitrogen (398.6 eV), pyrrolic nitrogen (399.8 eV), graphitic nitrogen (402.6 eV), and oxidised nitrogen (405.1 eV).[4]

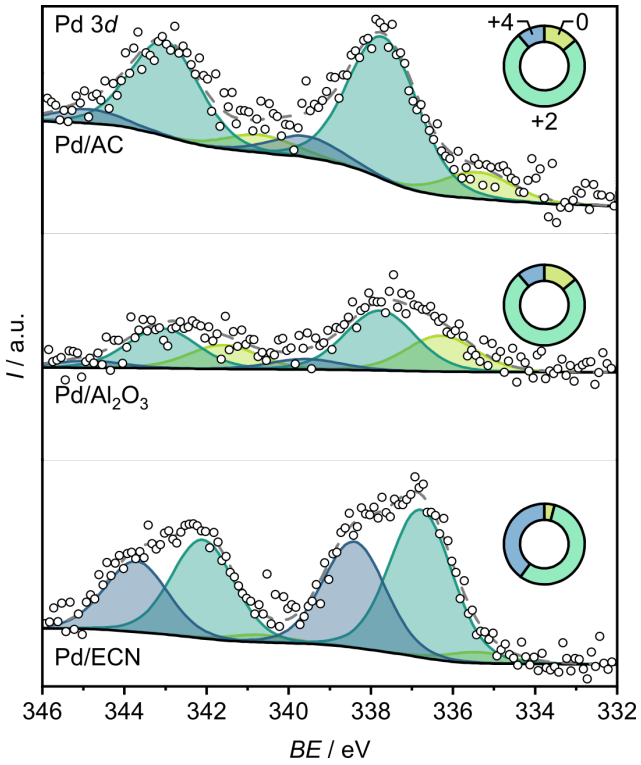

Fig. S6. Pd 3*d* XPS spectra and corresponding fits (dotted line) of the as-prepared Pd SACs. Shaded areas indicate spectral components corresponding to Pd^{4+}, Pd^{2+}, and Pd^{0} (relative contributions shown inset). As expected, all SACs evidenced predominantly positively charged palladium species. The reduced signal intensity in Pd/Al_2O_3 coincided with its lower metal content. The presence of a minor contribution of neutrally charged palladium, predominant for Pd/ECN, could either stem from small clusters or arise as an artefact of the fitting procedure.

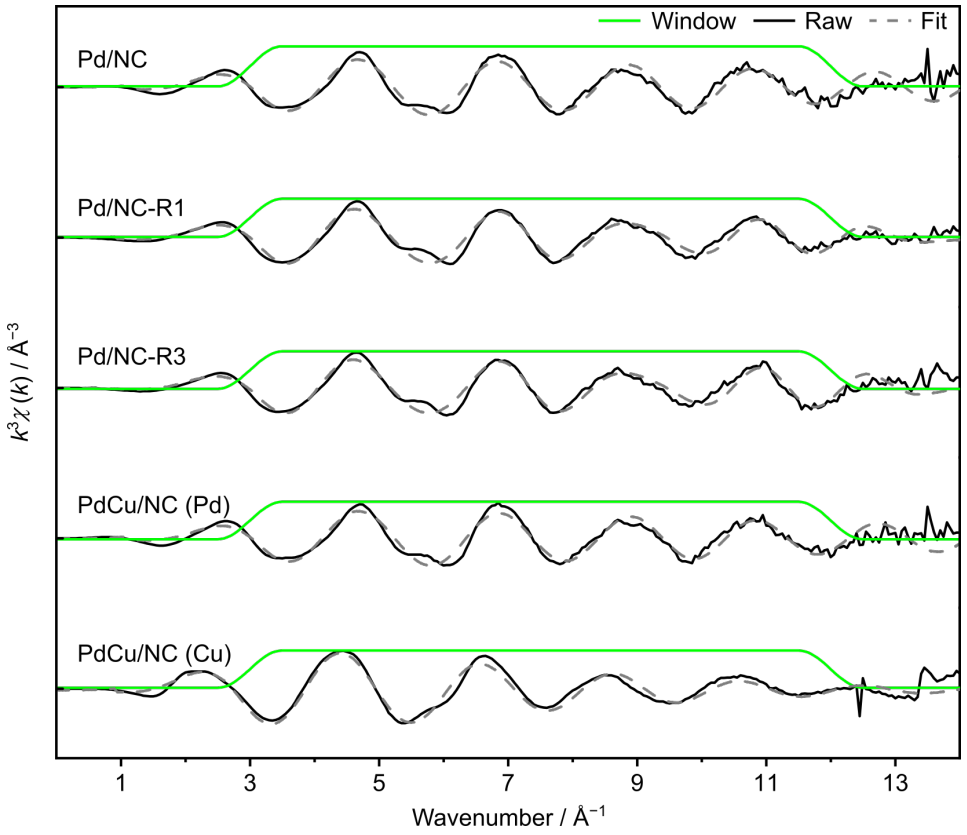

Fig. S7. EXAFS as a function of wavenumber of as-prepared and used (-R1-3) Pd/NC and PdCu/NC catalysts. Windows with *k*-values ranging from 3 to 12 Å^{-1} yielded the best data quality and were used for all fittings.

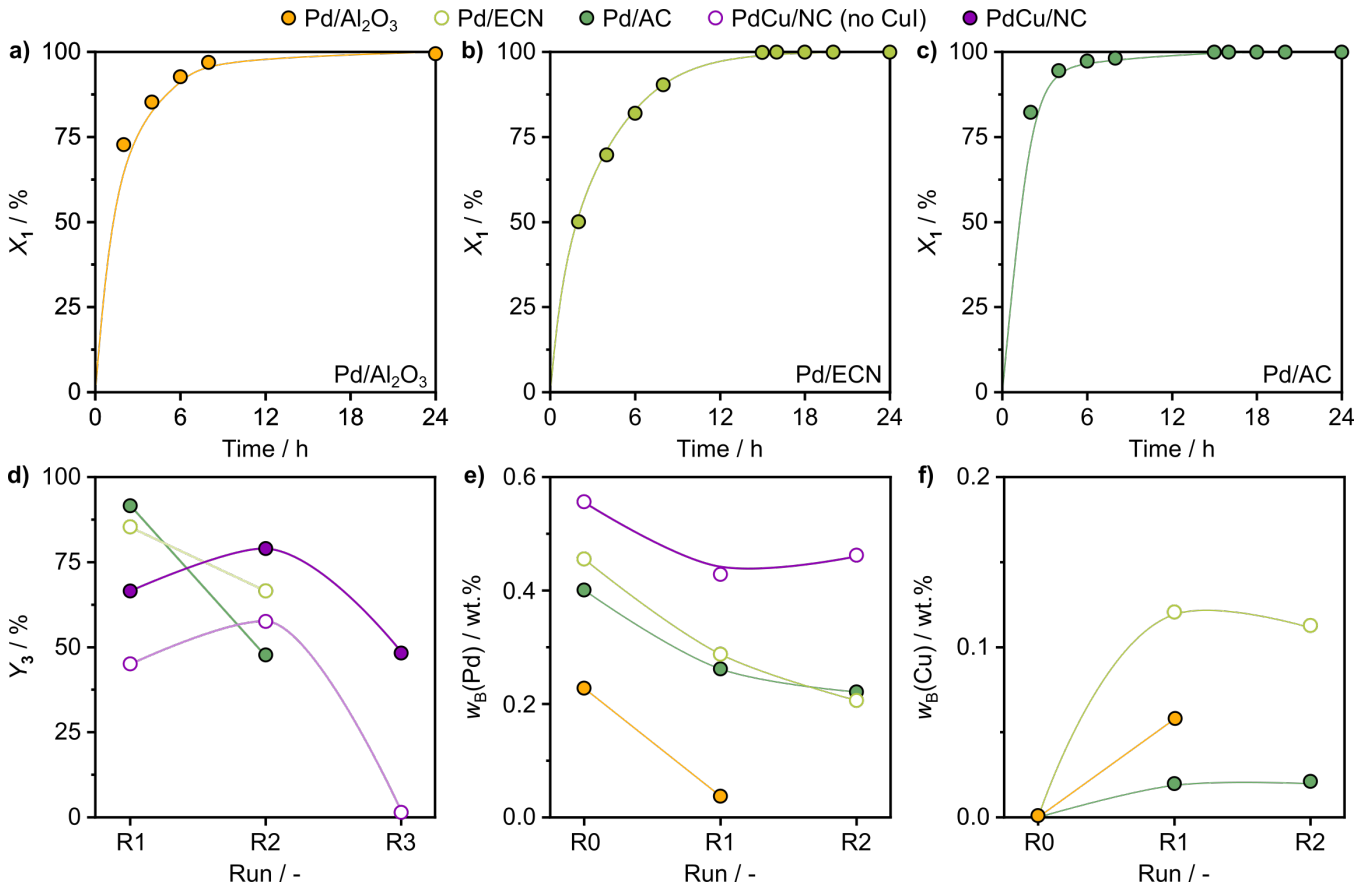

Fig. S8. Conversion of iodobenzene (X_1) over time in the Sonogashira coupling with phenylacetylene (**2**) using a) Pd/Al_2O_3, b) Pd/ECN, and c) Pd/AC. The activity of both Pd/AC and Pd/Al_2O_3 was similar to the homogeneous benchmarks (see Fig. 4c in the main text), Pd/ECN displayed a lower iodobenzene conversion, reaching 100% after approximately 16 h. d) Yield of the desired Sonogashira product **3** (Y_3) after consecutive runs (-R1-3) of Pd/ECN, Pd/AC, and PdCu/NC (kinetic profiles shown in Fig. 5 in the main text). The activity decrease observed from the first and second catalytic run (Pd/AC and Pd/ECN) may be caused by metal leaching. Differences between PdCu/NC operated in the presence and absence of CuI are likely caused by the abundance of soluble copper species. e) The evolution of bulk palladium content (w_B(Pd)) over consecutive catalytic tests (R0, as-prepared catalyst) confirmed a significant loss of metal during the first run for all of these carriers. f) Analysis of the used catalysts confirmed the presence of Cu (w_B(Cu)), likely owing to the adsorption of Cu species from the reaction medium (values for PdCu/NC shown in Table S5). The color codes shown in the legend apply to all panels. Standard reaction conditions: 353 K, 0.1 mol% Pd, 1 mol% CuI, 1 mol% PPh_3, 2 eq. NEt_3, 24 h (d-f).

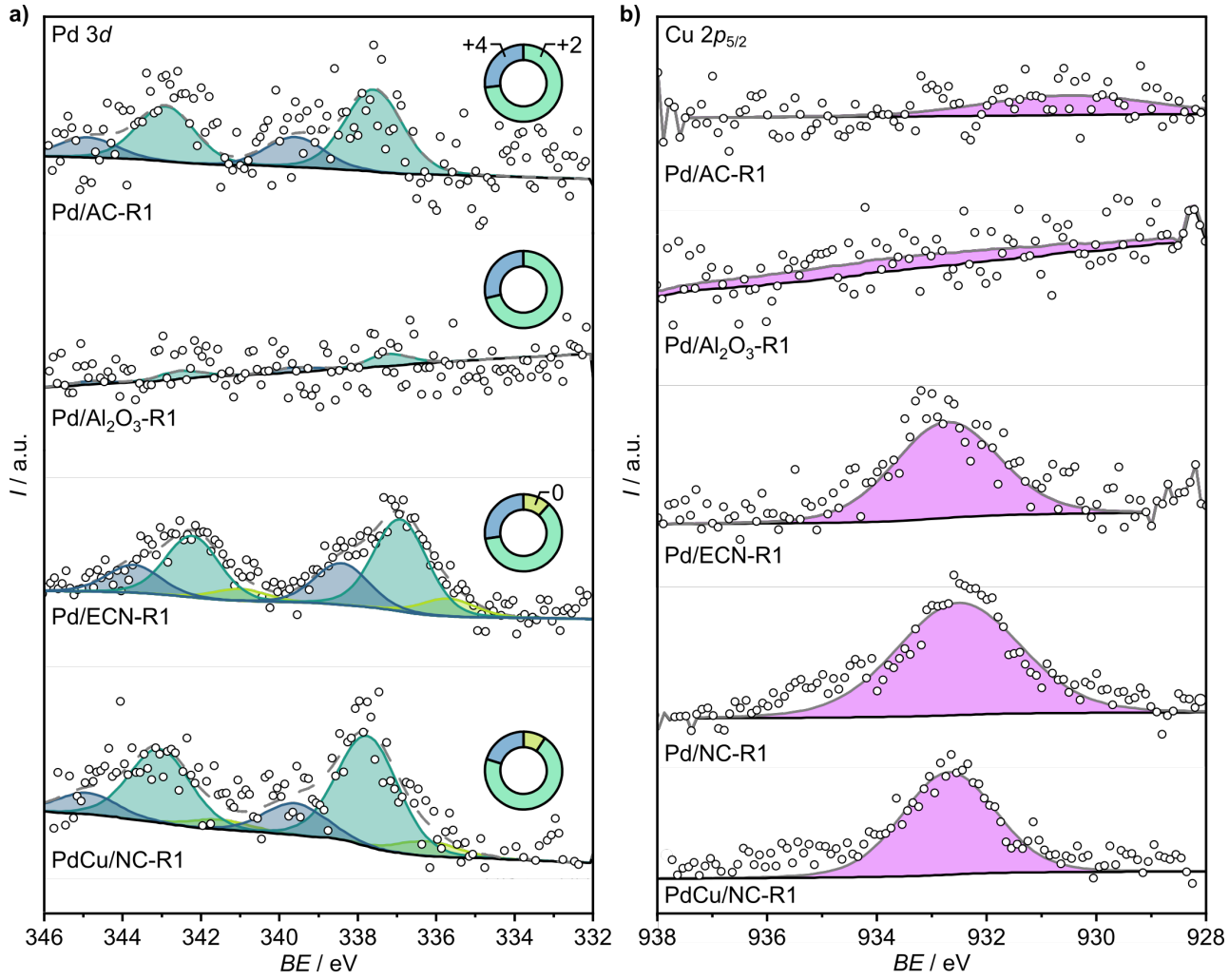

Fig. S9. a) Pd 3*p* and b) Cu $2p_{5/2}$ XPS spectra of the Pd SACs after one catalytic run (-R1). Shaded areas indicate spectral components corresponding to Pd^{4+}, Pd^{2+} and Pd^{0} (relative contributions shown inset). The share of Pd^{4+} in PdCu/NC-R1 decreased significantly in favour of Pd^{2+}. AC- and Al_2O_3-supported catalysts displayed low signal intensity of palladium, coinciding with the reduced bulk palladium content evidenced. Both, Pd/AC-R1 and Pd/Al_2O_3-R1 displayed negligible copper uptake. The Pd speciation in Pd/ECN-R1 was similar to the as-prepared catalyst. Pd/ECN-R1, Pd/NC-R1, and PdCu/NC-R1 evidenced a notable signal in the Cu $2p_{5/2}$ region related to Cu^{2+}.[7]

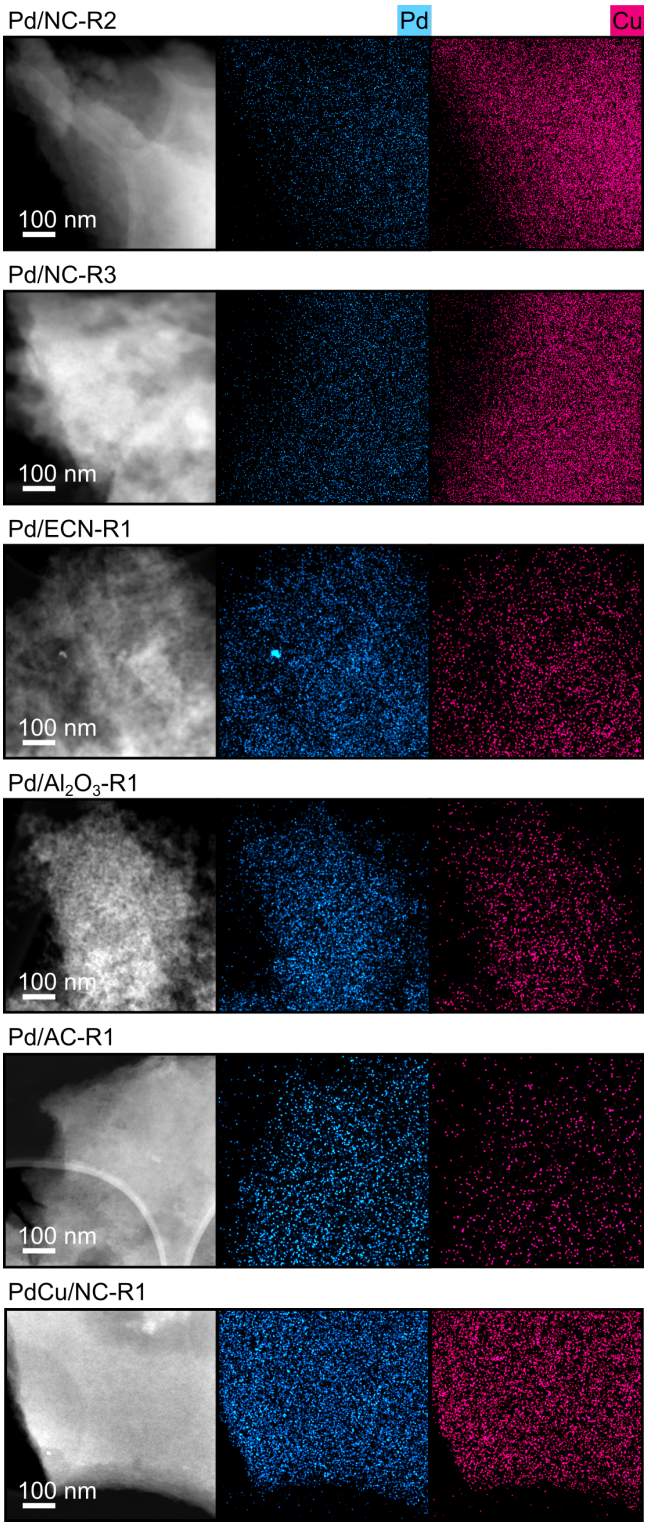

Fig. S10. HAADF-STEM images and EDX maps of the Pd SACs after different catalytic runs (-R1-3, respectively). No palladium nanoparticles were visible in the used catalyst except for Pd/ECN. Copper species were observed to be uniformly dispersed across all the samples.

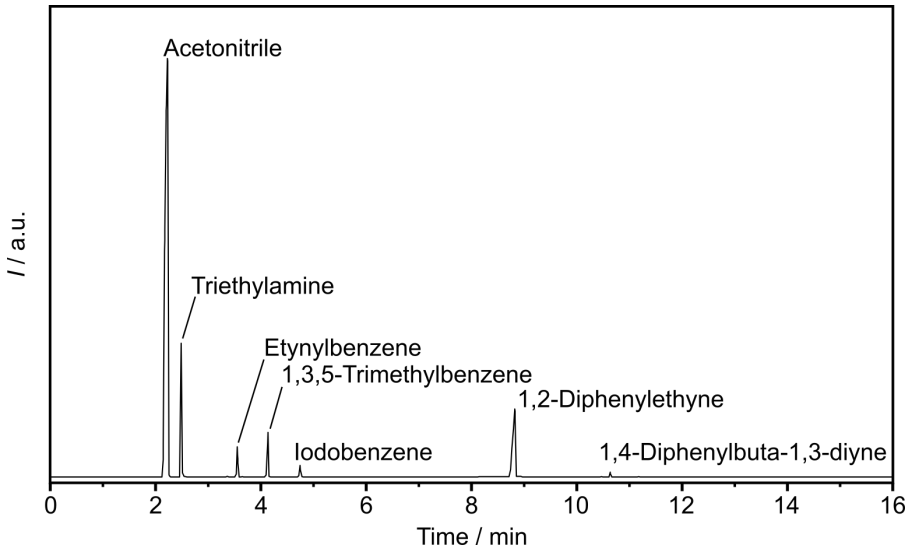

Fig. S11. Example gas chromatogram of the reaction aliquot after 24 h. Measurements were performed on a Thermo TRACE 1300 chromatograph equipped with a flame ionisation detector, and a ZB-5 column (5%-phenyl-95%-dimethylpolysiloxane, 30 m length, 0.25 mm inner diameter, 0.25 µm film thickness) and helium as carrier gas (split injection, flow: 0.8 cm^3 min^{-1}, split ratio: 125). Inlet and detector temperature were set to 573 K. The initial column temperature was set to 313 K and continuously increased to 320 K (heating rate 20 K min^{-1}, hold time 10 min).

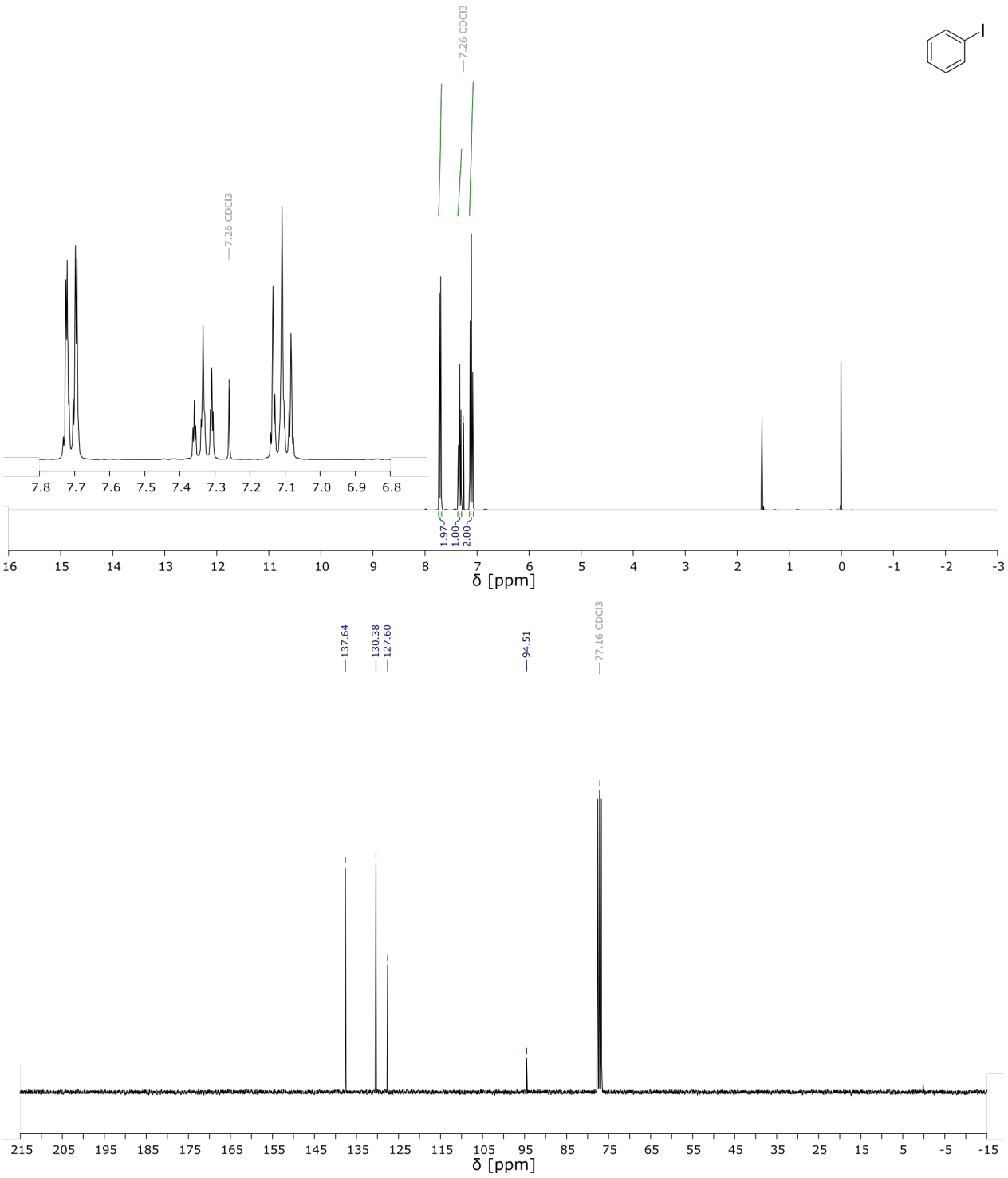

Fig. S12. ^{1}H- (top) and ^{13}C-NMR (bottom) spectra of iodobenzene (compound **1**).

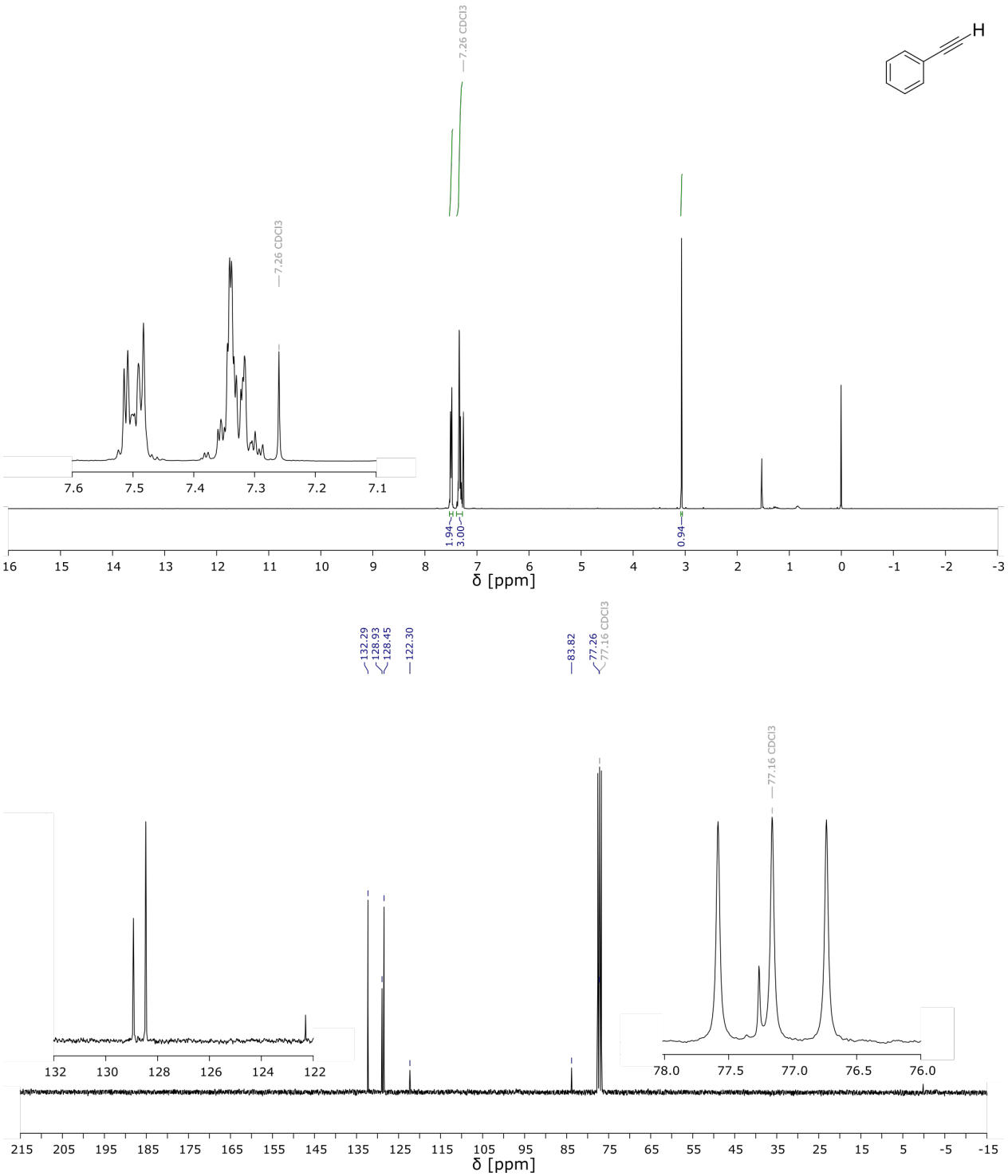

Fig. S13. ^{1}H- (top) and ^{13}C-NMR (bottom) spectra of ethynylbenzene (compound **2**).

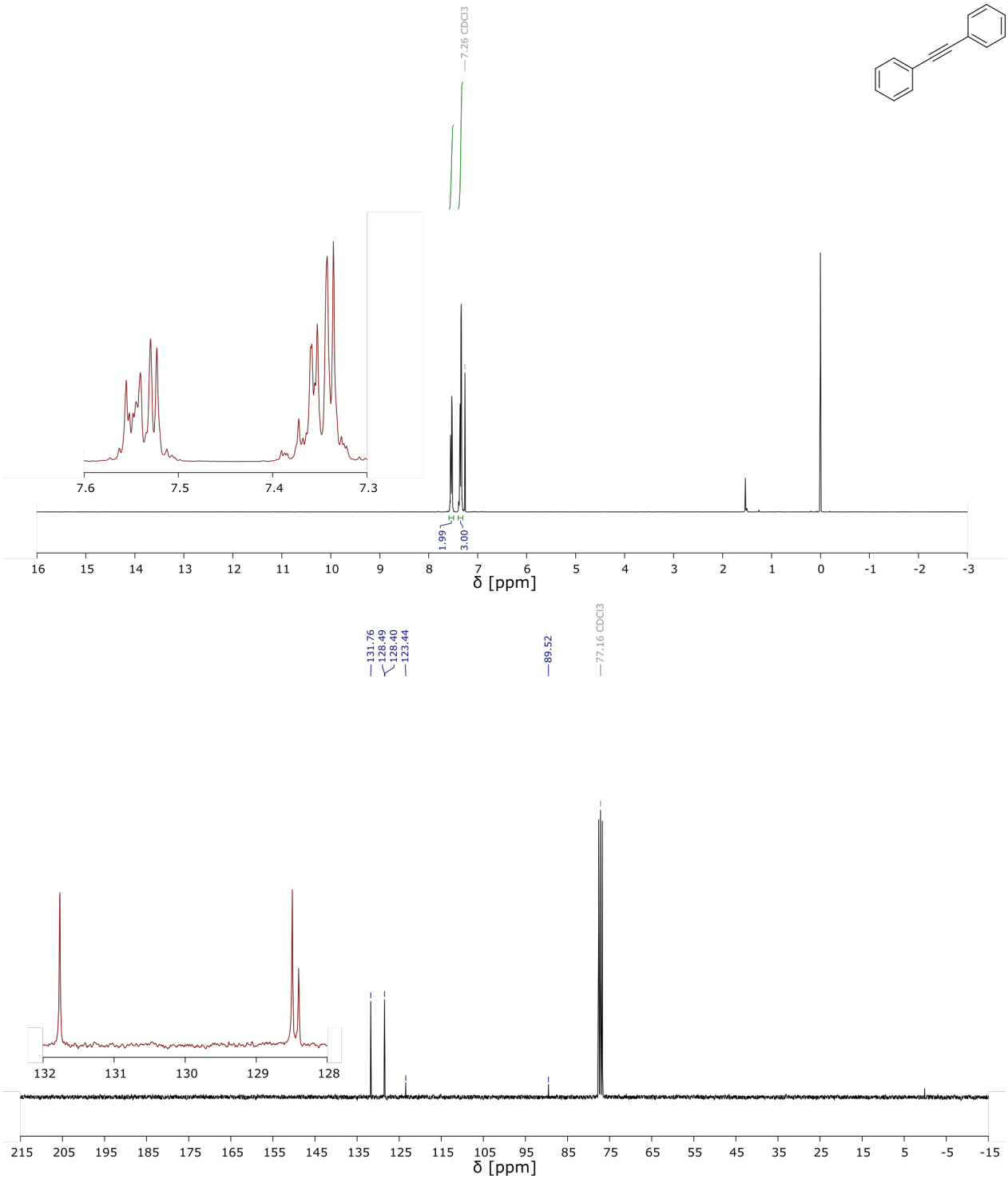

Fig. S14. ^{1}H- (top) and ^{13}C-NMR (bottom) spectra of 1,2-diphenylethyne (compound **3**).

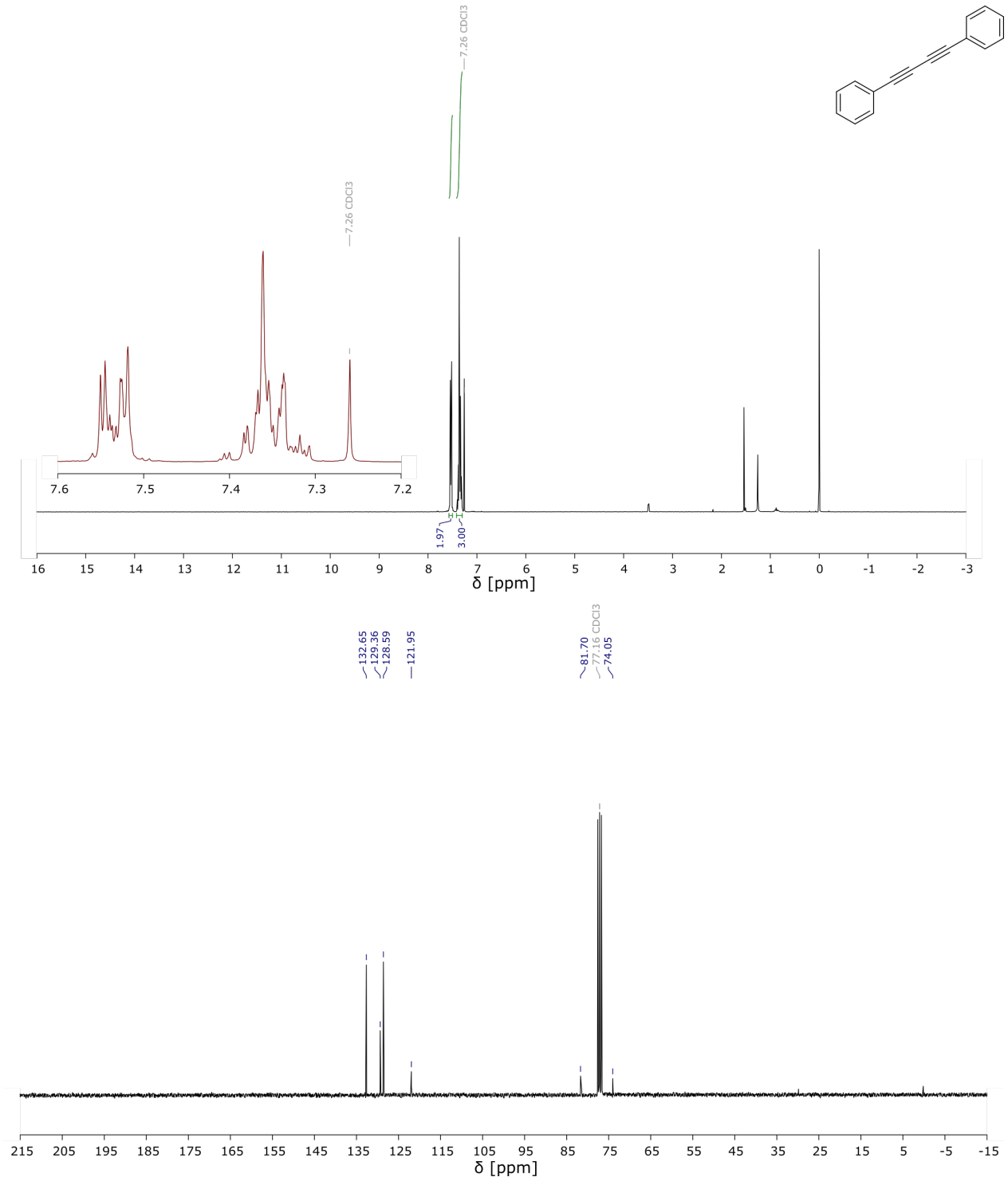

Fig. S15. ^{1}H- (top) and ^{13}C-NMR (bottom) spectra of 1,4-diphenylbuta-1,3-diyne (compound **4**).

Supplementary References

1 S. Büchele, Z. Chen, S. Mitchell, R. Hauert, F. Krumeich and J. Pérez-Ramírez, *ChemCatChem*, 2019, **11**, 2812-2820.

2 Z. Chen, S. Mitchell, E. Vorobyeva, R. K. Leary, R. Hauert, T. Furnival, Q. M. Ramasse, J. M. Thomas, P. A. Midgley, D. Dontsova, M. Antonietti, S. Pogodin, N. López and J. Pérez-Ramírez, *Adv. Funct. Mater.*, 2017, **27**, 1605785.

3 P. J. Schmitz, K. Otto and J. E. de Vries, *Appl. Catal., A*, 1992, **92**, 59-72.

4 R. Lin, S. K. Kaiser, R. Hauert and J. Pérez-Ramírez, *ACS Catal.*, 2018, **8**, 1114-1121.

5 C. Ronning, H. Feldermann, R. Merk, H. Hofsäss and P. Reinke, *Phys. Rev. B - Condens. Matter Mater. Phys.*, 1998, **58**, 2207-2215.

6 N. Hellgren, R. T. Haasch, S. Schmidt, L. Hultman and I. Petrov, *Carbon*, 2016, **108**, 242-252.

7 M. C. Biesinger, *Surf. Interface Anal.*, 2017, **49**, 1325-1334.

8 N. Fairley, V. Fernandez, M. Richard-Plouet, C. Guillot-Deudon, J. Walton, E. Smith, D. Flahaut, M. Greiner, M. Biesinger, S. Tougaard, D. Morgan and J. Baltrusaitis, *Appl. Surf. Sci. Adv.*, 2021, **5**, 100112.

9 B. Ravel and M. Newville, *J. Synchrotron Radiat.*, 2005, **12**, 537-541.

10 ISO 14044:2006: Environmental management - Life Cycle Assessment: Requirements and guidelines, https://www.iso.org/standard/38498.html, (accessed February 2022).

11 E. Vorobyeva, Z. Chen, S. Mitchell, R. K. Leary, P. Midgley, J. M. Thomas, R. Hauert, E. Fako, N. López and J. Pérez-Ramírez, *J. Mater. Chem. A*, 2017, **5**, 16393–16403.

12 C. Ronning, H. Feldermann, R. Merk, H. Hofsäss and P. Reinke, *Phys. Rev. B - Condens. Matter Mater. Phys.*, 1998, **58**, 2207–2215.